2006-03-20

Effect of CO on NO and N2O Conversions in Nonthermal Argon Plasma

Morris D. Argyle
Brigham Young University, mdargyle@byu.edu

Gui-Bing Zhao

Maciej Radosz

Original Publication Citation

G.B. Zhao, M.D. Argyle, M. Radosz, "Effect of CO on NO and N2O Conversion in Nonthermal Argon Plasma." Journal of Applied Physics, 99, 11332/1-11332/14, 26. http://jap.aip.org/resource/1/japiau/v99/i11/p11332_s1

Effect of CO on NO and N2O conversions in nonthermal argon plasma

Gui-Bing Zhao, Morris D. Argyle, and Maciej Radosz

Citation: J. Appl. Phys. **99**, 113302 (2006); doi: 10.1063/1.2197067
View online: http://dx.doi.org/10.1063/1.2197067
View Table of Contents: http://jap.aip.org/resource/1/JAPIAU/v99/i11
Published by the American Institute of Physics.

Effect of CO on NO and N_2O conversions in nonthermal argon plasma

Gui-Bing Zhao,[a] Morris D. Argyle,[b] and Maciej Radosz[c]
Department of Chemical and Petroleum Engineering, College of Engineering, University of Wyoming, Laramie, Wyoming 82071-3295

(Received 8 September 2005; accepted 20 March 2006; published online 2 June 2006)

200–600 ppm of CO inhibit NO conversion in nonthermal Ar plasma, but do not produce N_2O. However, 1.01% of CO has no effect on NO conversion, but produces N_2O. In general, N_2O conversion in Ar plasma decreases with increasing CO concentration. These experimental results cannot be explained by charge transfer reactions of Ar^+. Selectivity analysis of all excited states of Ar possibly contributing to NO_x conversion without and with CO suggests that only $Ar(^3P_2)$ contributes to NO_x conversion and CO dissociation. A kinetic model of 43 reactions is required to model NO conversion or N_2O conversion in Ar without CO, whereas 81 reactions are required to model NO conversion and N_2O conversion in Ar with CO. At constant gas pressure, a single set of model parameters can predict NO conversion or N_2O conversion without and with CO. All experimental results can be explained using a reaction mechanism in which excited neutral states of Ar are the only active species, which supports the conclusion that cations have a negligible impact on these nonthermal plasma reactions. © *2006 American Institute of Physics*.
[DOI: 10.1063/1.2197067]

I. INTRODUCTION

Implementation of environmental regulations governing the emission of harmful gases, such as NO_x, requires efficient abatement methods. Among the emerging technologies for NO_x conversion, nonthermal plasma is one of the most promising. A pulsed corona discharge reactor (PCDR) is one of these nonthermal plasma technologies, characterized by low gas temperature and high electron temperature, achieved by producing high energy electrons in the gas while leaving the bulk temperature of the gas unchanged. A PCDR employs a high-voltage, short-duration (<100 ns) electrical discharge between nonuniform electrodes to produce streamers through the growth of electron avalanches formed by electron collision ionization events. A streamer is a region of partly ionized gas, where metastable excited states, radicals, and ions are formed through electron collision reactions with the background gas. These chemically active species, in turn, initiate bulk phase reactions that lead to NO_x conversion to nitrogen and oxygen.

Understanding the formation of the chemically reactive species and their reaction pathways is essential to optimize nonthermal plasma processing for practical application. The role of cations on NO_x conversion has been debated. For example, Chang[1] compared the rate constants of charge transfer reactions and radical reactions and concluded that, because the cationic reaction probabilities are a few orders of magnitude larger than radical reactions, the charge transfer reactions of cations play an important role in de-NO_x processes. In contrast, on the basis of extensive experimental and theoretical experiences, Kogelschatz[2] proposed that charged particle reactions are negligible in ambient-pressure nonthermal plasma, and neutral active species, such as atoms, molecular fragments, and excited molecules, are the major active species contributing to nonthermal plasma reactions. Van Veldhuizen *et al.*[3] analyzed the relative importance of ions and radicals for NO conversion in a pulsed corona reactor and showed that the ion contribution to NO conversion is on the order of 10%–20% of the radical contribution. However, on the basis of this conclusion, their calculated NO conversion was 10–100 times lower than the experimental values. Recently, Hu *et al.*[4] proposed that both N_2^+ cations and N radicals are responsible for NO_x (NO, NO_2, and N_2O) conversion in nonthermal N_2 plasma. However, their reaction mechanism did not predict by-product N_2O concentrations in NO/N_2 mixtures or by-product NO concentrations in NO_2/N_2 mixtures. Later, Zhao *et al.*[5,6] found that only two active species, the first excited state of molecular nitrogen, $N_2(A\ ^3\Sigma_u^+)$, and N radicals, are responsible for NO_x conversion in nonthermal N_2 plasma and that N_2^+ does not contribute to NO_x conversion. Using the reaction mechanism including $N_2(A\ ^3\Sigma_u^+)$ and N radicals without cations, Zhao *et al.*[5,6] predicted all their experimental data, which confirmed that N_2^+ does not contribute to NO_x conversion. The reaction mechanism that includes the neutral active species (excited states and radicals) and excludes ions can explain the effect of CO, O_2, and CO_2 on NO_x conversion in nonthermal nitrogen plasma.[5,7–9] More recently, by analyzing corona induced optical emissions and the mechanism of streamer discharge, Zhao *et al.*[10] found that charge transfer reactions of cations have a negligible contribution to NO_x conversion in nonthermal plasma.

The multitude of chemically active species produced in the streamer through electron collision reactions with the background gas leads to complex reaction mechanisms in nonthermal plasma, especially for multiple component systems. However, the reaction mechanism must be self-consistent for all reactant systems to which it is applied. For

[a]Electronic mail: gbzhao@uwyo.edu
[b]Electronic mail: mdargyle@uwyo.edu
[c]Electronic mail: radosz@uwyo.edu

example, if conversion of low (ppm) concentrations of NO_x in nonthermal argon plasmas can be explained using reactions involving cations, such as Ar^+, the same active species should be involved in NO_x conversion in Ar in the presence of CO. However, Hu *et al.*[11] found that the reaction mechanism based on Ar^+ can describe NO_x conversion in Ar, but not the effect of CO on NO_x conversion in Ar. This prompts us to revisit the role of Ar^+ as a dominant active species contributing to NO_x conversion in nonthermal Ar plasma.

The goal of this work, therefore, is to explore a self-consistent reaction mechanism involving argon excited states that could explain the effect of CO on NO and N_2O conversions in nonthermal argon plasma. The reasons for choosing Ar as the balance gas instead of gases commonly found in NO_x containing streams, such as nitrogen, oxygen, water, and CO_2,[3,12] are explained elsewhere.[3,12] Briefly, argon forms more cations than the other gases, which helps understand the importance of ion transfer reactions, and argon produces fewer, less complex active species that are easier to analyze.

II. EXPERIMENTAL SECTION

The experimental apparatus and measurement procedures are described in detail elsewhere.[11,13] In brief overview, the pulsed corona discharge reactor used in this work consists of a high-voltage power supply and a pulser/reactor assembly. The pulser/reactor assembly contains a pulsed power generator and pulsed corona discharge tubes. The reactor has UV-grade quartz windows for diagnostics and plasma observation and ten parallel stainless steel tubes, each 914 mm in length and 23 mm in diameter, with a stainless steel wire, 0.58 mm in diameter, passing axially through the center of each tube. In all of the experiments described in this work, only four of ten tubes are wired and used, and the remaining six tubes are sealed with Teflon corks with O-rings. The wire is positively charged and the tube is grounded. The energy delivered to the reactor per pulse is calculated from $(1/2)CV_c^2$, where C is the pulse forming capacitance (800 pF in this work) and V_c is charge voltage in the pulse forming capacitance before discharge.[7,14] The power consumed, W (J s^{-1}), is calculated as the product of the input energy per pulse and the pulse frequency.

The experimental conditions are summarized in Table I. The certified feed gas mixtures of low (ppm) concentration nitrogen oxides in argon with and without CO shown in Table I are used as supplied (Airgas, Inc.). The feed gas mixture, maintained at ambient temperature, around 300 K, is fed through the PCDR at two flow rates (measured at the reactor inlet conditions) of 3.45×10^{-4} m^3 s^{-1} at 141 kPa and 4.01×10^{-4} m^3 s^{-1} at 189 kPa. The feed samples and the reactor effluent samples, collected in small stainless steel cylinders, are analyzed for stable species with a Spectrum 2000 Perkin Elmer Fourier transform infrared (FTIR) spectrometer with a narrow band mercury cadmium telluride (MCT) detector, as reported previously.[5–9,13–15] For all experimental data, nitrogen oxides other than NO, NO_2, and N_2O are not detected by FTIR, which has a detection limit of 5 ppm for each of these species. All experimental data are reproducible within a ±10% error limit, including the FTIR and flow measurement uncertainties.

TABLE I. Experimental matrix.

System	Flow rate (m^3 s^{-1})	Reactor pressure (kPa)
NO in Ar		
314 ppm NO	3.45×10^{-4}	141[a]
414 ppm NO	3.45×10^{-4}	141[a]
570 ppm NO	3.45×10^{-4}	141[a]
314 ppm NO	4.01×10^{-4}	189
414 ppm NO	4.01×10^{-4}	189
570 ppm NO	4.01×10^{-4}	189[a]
N_2O in Ar		
290 ppm N_2O	3.45×10^{-4}	141[a]
217 ppm N_2O	3.45×10^{-4}	141[a]
105 ppm N_2O	3.45×10^{-4}	141[a]
47.6 ppm N_2O	3.45×10^{-4}	141[a]
217 ppm N_2O	4.01×10^{-4}	189[a]
105 ppm N_2O	4.01×10^{-4}	189
47.6 ppm N_2O	4.01×10^{-4}	189[a]
NO plus CO in Ar		
411 ppm NO+203 ppm CO	3.45×10^{-4}	141[a]
396 ppm NO+435 ppm CO	3.45×10^{-4}	141[a]
426 ppm NO+619 ppm CO	3.45×10^{-4}	141[a]
575 ppm NO+1.01% CO	3.45×10^{-4}	141
577 ppm NO+1.01% CO	4.01×10^{-4}	189
440 ppm NO+1.01% CO	4.01×10^{-4}	189
N_2O plus CO in Ar		
293 ppm N_2O plus 197 ppm CO	3.45×10^{-4}	141[a]
292 ppm N_2O+305 ppm CO	3.45×10^{-4}	141[a]
273 ppm N_2O+389 ppm CO	3.45×10^{-4}	141[a]
50.7 ppm N_2O+1.01% CO	4.01×10^{-4}	189[a]
103 ppm N_2O+1.01% CO	4.01×10^{-4}	189
215 ppm N_2O+1.01% CO	4.01×10^{-4}	189[a]

[a]Experimental data originally reported in Ref. 11.

A lumped kinetic model used to describe the concentrations of all species in the PCDR is reported elsewhere.[6]

III. RESULTS AND DISCUSSION

A. Experimental observations

In all experiments with CO, the CO concentration is relatively stable and does not vary by more than 40 ppm. Figure 1 shows the effect of CO on NO conversion in nonthermal argon plasma at a flow rate of 3.45×10^{-4} m^3 s^{-1} and 141 kPa. Figure 1(a) compares concentrations of NO, NO_2, and N_2O as a function of power input for NO inlet concentrations of ~411 ppm with and without 203 ppm CO. In both cases, NO_2 is the only by-product and N_2O is not detected. NO and NO_2 concentrations with 203 ppm CO are higher than those without CO at the same power input, which indicates that NO conversion to N_2 and O_2 is reduced by low concentrations of CO, as shown in Fig. 1(b). NO conversion is defined as

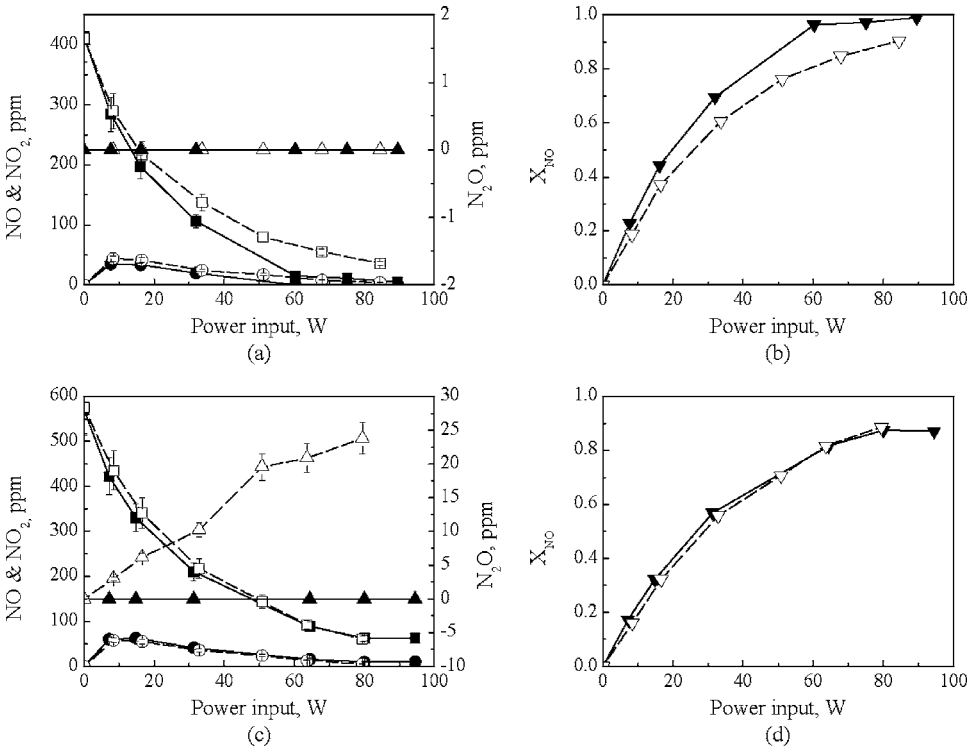

FIG. 1. Effect of CO on NO conversion in nonthermal argon plasma at a flow rate of 3.45×10^{-4} m^3 s^{-1} and 141 kPa. (a) Concentration of NO, NO_2, and N_2O as a function of power input: 414 ppm NO in Ar, (■) NO, (●) NO_2, and (▲) N_2O; 411 ppm NO plus 203 ppm CO in Ar, (□) NO, (○) NO_2, and (△) N_2O. (b) NO conversion as a function of power input: (▼) 414 ppm NO in Ar and (▽) 411 ppm NO plus 203 ppm CO in Ar. (c) Concentration of NO, NO_2, and N_2O as a function of power input: 570 ppm NO in Ar, (■) NO, (●) NO_2, and (▲) N_2O; 575 ppm NO plus 1.01% CO in Ar, (□) NO, (○) NO_2, and (△) N_2O. (d) NO conversion as a function of power input: (▼) 570 ppm NO in Ar and (▽) 575 ppm NO plus 1.01% CO in Ar.

$$X_{\mathrm{NO}} = \frac{C_{i,\mathrm{NO}} - C_{o,\mathrm{NO}} - C_{o,\mathrm{NO_2}}}{C_{i,\mathrm{NO}}}, \tag{1}$$

where C_i is the concentration of the given species at the reactor inlet, C_o is the concentration at the reactor outlet, and X_{NO} is the conversion of NO to N_2 and N_2O (with NO_2 formation excluded from NO conversion). In the present experiment, N_2O concentrations are zero. The results in Fig. 1(b) show that 203 ppm of CO inhibit NO conversion. Similar results were obtained by comparing other experimental data sets (414 ppm NO in Ar to 396 ppm NO plus 435 ppm CO in Ar and 426 ppm NO plus 619 ppm CO in Ar at the same flow rate and reactor pressure).

Figure 1(c) compares concentrations of NO, NO_2, and N_2O as a function of power input for NO inlet concentrations of ~570 ppm with and without 1.01% CO at 3.45×10^{-4} m^3 s^{-1} and 141 kPa. At this higher CO concentration, N_2O is detected, while without CO, N_2O is again not detected. NO and NO_2 concentrations with 1.01% CO are almost the same as those without CO at the same power input, which indicates that NO conversion to N_2, O_2, and N_2O is not affected by high (1.01%) CO concentrations, as confirmed in Fig. 1(d). Similar results were obtained for the same concentrations at higher flow rates (4.01×10^{-4} m^3 s^{-1}) and pressures (189 kPa).

Figure 2 shows the effect of CO on N_2O conversion in nonthermal argon plasma. For N_2O conversion in Ar with or without CO, N_2O is the only oxide of nitrogen detected by FTIR, which indicates that N_2O is directly converted into N_2 and O_2. N_2O conversion is defined as

$$X_{\mathrm{N_2O}} = \frac{C_{i,\mathrm{N_2O}} - C_{o,\mathrm{N_2O}}}{C_{i,\mathrm{N_2O}}}, \tag{2}$$

where $X_{\mathrm{N_2O}}$ is the conversion of N_2O to N_2 and O_2, and C_i and C_o are the respective N_2O concentrations at the reactor inlet and outlet. Figure 2(a) compares N_2O concentration and conversion as a function of power input without and with 305 ppm CO for N_2O inlet concentrations of ~290 ppm at 3.45×10^{-4} m^3 s^{-1} and 141 kPa. At the same power input, N_2O concentration with 305 ppm CO is higher than that without CO, resulting in lower N_2O conversion, which indicates that low (ppm) concentrations of CO also inhibit N_2O conversion. Similar results were obtained at other low inlet

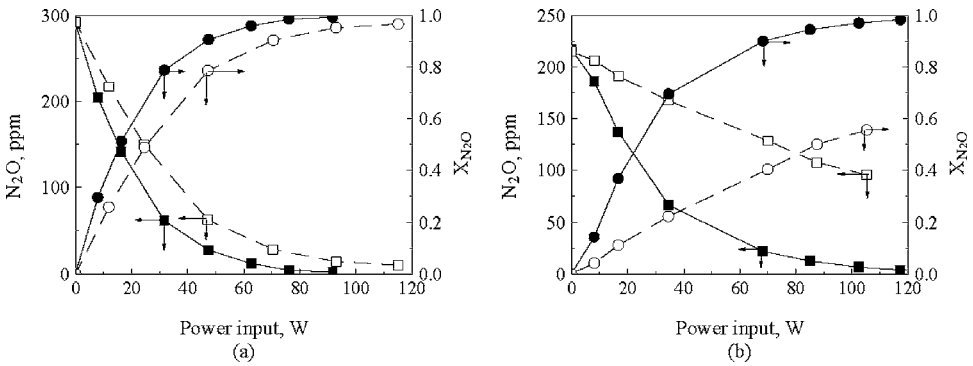

FIG. 2. Effect of CO on N_2O conversion in nonthermal argon plasma. (a) N_2O concentration and N_2O conversion as a function of power input at a flow rate of 3.45×10^{-4} m^3 s^{-1} and 141 kPa. Filled symbols: 290 ppm N_2O in Ar; open symbols: 292 ppm N_2O plus 305 ppm CO in Ar. (b) N_2O concentration and N_2O conversion as a function of power input at a flow rate of 4.01×10^{-4} m^3 s^{-1} and 189 kPa. Filled symbols: 217 ppm N_2O in Ar; open symbols: 215 ppm N_2O plus 1.01% CO in Ar.

N_2O concentration experimental conditions (290 ppm N_2O in Ar compared with 293 ppm N_2O plus 197 ppm CO in Ar and 273 ppm N_2O plus 389 ppm CO in Ar at the same flow rate and reactor pressure).

Figure 2(b) compares N_2O concentrations and conversion as a function of power input without and with 1.01% CO for inlet N_2O concentrations of ~215 ppm at 4.01×10^{-4} m^3 s^{-1} and 189 kPa. High concentrations (1.01%) of CO strongly inhibit N_2O conversion. Similar results were obtained at other experimental conditions (105 ppm N_2O in Ar compared with 103 ppm N_2O plus 1.01% CO in Ar and 47.6 ppm N_2O in Ar compared with 50.7 ppm N_2O plus 1.01% CO in Ar at the same flow rates and reactor pressures.

Comparison of Figs. 1(a) and 1(b) with Figs. 1(c) and 1(d) indicates that low (ppm) concentrations of CO inhibit NO conversion, but high (percent) concentrations of CO do not. N_2O is formed in detectable quantities only when high concentrations of CO are present with NO in Ar. Comparison of Figs. 2(a) and 2(b) indicates that N_2O conversion decreases with increasing CO concentrations. These experimental observations cannot be explained by reaction mechanisms involving charge transfer reactions of Ar^+, as reported recently by Hu *et al.*[11]

B. Electron collision reactions

Electrons generated by the electrical discharge collide with gas molecules to produce chemically active species, such as radicals, atoms and molecules in excited electronic states, and ions, which trigger NO_x reactions.[16] Previous investigations have shown that Ar^+ has a negligible contribution to NO_x conversion in Ar plasma[10] and that the reaction mechanism involving Ar^+ cannot explain the effect of CO on NO_x conversion.[11] Therefore, reactions with ions are not considered in this analysis.

In all experiments shown in Table I, the major stable species in the PCDR are Ar, NO_x, N_2, O_2, CO, and CO_2. In most cases, electron collision reactions with a given species are negligible if the concentration of that species in the PCDR is less than 1000 ppm.[6,7,9,16] Therefore, electron interactions with NO_x, N_2, O_2, and CO_2 are not considered because concentrations of these species are always less than 1000 ppm. For low (ppm) CO concentrations, electron collision reactions with CO are also negligible. Previous investigations[7,9] on the effect of ~1% concentrations of O_2 and CO_2 on NO_x conversion in N_2 plasma showed that electron collision reactions with O_2 or CO_2 cannot be neglected, relative to electron collision reactions with N_2, because the dissociation energies of O_2 and CO_2 are far lower than those of N_2. This result implies that electron collision reactions with CO cannot be neglected at 1.01% CO concentration.

Electron collision reactions with CO mainly contribute to CO molecular excitation and dissociation in the following reactions:

$$e + \mathrm{CO} \rightarrow \mathrm{CO}^* + e, \tag{3}$$

$$e + \mathrm{CO} \rightarrow \mathrm{C} + \mathrm{O} + e, \tag{4}$$

where CO^* represents excited states of CO that include $a\,^3\Pi$, $a'^3\Sigma^+$, $d\,^3\Delta$, $e\,^3\Sigma^-$, and $A\,^1\Pi$.[17] These excited states may return to the ground state by radiative emission, interaction with Ar or other CO molecules (quenching reactions), or by interaction with NO_x (generally resulting in NO_x conversion reactions). All of the CO excited states have quenching rate constants of at least 2.11×10^{12} cm^3 mol^{-1} s^{-1} with Ar or CO and reaction rate constants of at most 1.66×10^{14} cm^3 mol^{-1} s^{-1} with NO_x.[17] These values imply that the CO excited states produced are quenched to the ground state by argon (or relax by radiative emission) and hence do not contribute significantly to NO_x conversion because the concentration of Ar is at least three orders of magnitude higher than that of NO_x. Thus, the quenching reaction rates are at least ten times higher than the reaction rates with NO_x. In addition, CO dissociation by electron collision (4) is unlikely to be significant because the dissociation energy of CO is high[18] (10.8 eV/CO) and the CO concentration is low in comparison with Ar. These conjectures are confirmed by the modeling results described later. Therefore, electron collision reactions with Ar are the only ones considered in this work.

A selectivity analysis[5,7,9] at the reactor inlet concentrations is used to identify the chemically active species produced by the electron collision reactions with Ar that are important in NO_x formation and conversion. Recent optical emission measurements[10] in nonthermal argon plasma demonstrated that there are 14 chemically active excited states of Ar formed by electron collision reactions, including four $3p^5\,4s$ configurations ($^3P_2$, $^3P_1$, $^3P_0$, and $^1P_1$) and ten $3p^5\,4p$ configurations ($2p_{10}$, $2p_9$, $2p_8$, $2p_7$, $2p_6$, $2p_5$, $2p_4$, $2p_3$, $2p_2$, and $2p_1$, using Paschen notation[19–22] instead of term symbols). Balamuta and Golde[23,24] showed that the lowest energy excited state of Ar, Ar($^3P_2$), can dissociate almost all oxygen-containing compounds including CO and NO_x. This implies that all 14 excited states of Ar formed in the PCDR could contribute to CO dissociation and NO_x conversion. These chemically active excited states may be consumed by four parallel processes: (1) natural radiation with accompanying optical emission, (2) quenching by the Ar background gas, (3) reaction with NO_x (conversion of NO_x), and (4) CO dissociation. As reported recently,[8,9] the selectivities of these four parallel processes can be defined as

$$S_I = \frac{R_I}{R_I + R_q + R_r + R_d} = \frac{k_I}{k_I + k_q C_{\mathrm{Ar}} + k_r C_{\mathrm{NO}_x} + k_d C_{\mathrm{CO}}} \times 100\,\%, \tag{5a}$$

$$S_q = \frac{R_q}{R_I + R_q + R_r + R_d} = \frac{k_q C_{\mathrm{Ar}}}{k_I + k_q C_{\mathrm{Ar}} + k_r C_{\mathrm{NO}_x} + k_d C_{\mathrm{CO}}} \times 100\,\%, \tag{5b}$$

$$S_r = \frac{R_r}{R_I + R_q + R_r + R_d} = \frac{k_r C_{\mathrm{NO}_x}}{k_I + k_q C_{\mathrm{Ar}} + k_r C_{\mathrm{NO}_x} + k_d C_{\mathrm{CO}}} \times 100\,\%, \tag{5c}$$

TABLE II. Initial selectivity of active species consumption in nonthermal argon plasma without CO by radiation, quenching, and NO conversion.

Ar excited states	k_I[a] (s^{-1})	$k_q C_{Ar}$[b] (s^{-1})	$k_r C_{NO_x}$[c] (s^{-1})	S_I (%)	$S_{q,Ar}$ (%)	S_{r,NO_x} (%)
$^3P_2$	2.63×10^{-2}	6.97×10^{6}	4.47×10^{6}	~0	60.9	39.1
$^3P_1$	1.05×10^{8}	9.44×10^{6}	6.53×10^{6}	86.8	7.80	5.40
$^3P_0$	2.23×10^{-2}	9.75×10^{6}	5.11×10^{6}	~0	65.6	34.4
$^1P_1$	4.00×10^{8}	4.73×10^{6}	1.10×10^{7}	96.2	1.1	2.6
$2p_{10}$	2.47×10^{7}	6.79×10^{8}	⋯	3.5	96.5	⋯
$2p_9$	3.26×10^{7}	1.09×10^{9}	9.38×10^{6}	2.9	96.3	0.8
$2p_8$	3.27×10^{7}	1.09×10^{9}	9.38×10^{6}	2.9	96.3	0.8
$2p_7$	3.31×10^{7}	2.61×10^{9}	⋯	1.3	98.7	⋯
$2p_6$	3.40×10^{7}	1.22×10^{9}	1.02×10^{7}	2.7	96.5	0.8
$2p_5$	4.10×10^{7}	1.60×10^{9}	1.02×10^{7}	2.5	96.9	0.6
$2p_4$	3.41×10^{7}	1.19×10^{9}	⋯	2.8	97.2	⋯
$2p_3$	3.45×10^{7}	1.05×10^{9}	⋯	3.2	96.8	⋯
$2p_2$	3.53×10^{7}	6.45×10^{8}	⋯	5.2	94.8	⋯
$2p_1$	4.61×10^{7}	1.36×10^{9}	1.59×10^{7}	3.2	95.6	1.1

[a]References 34–38.
[b]References 19–22.
[c]References 39 and 40.

$$S_d = \frac{R_d}{R_I + R_q + R_r + R_d} = \frac{k_d C_{CO}}{k_I + k_q C_{Ar} + k_r C_{NO_x} + k_d C_{CO}} \times 100\,\%\,, \tag{5d}$$

where S_I, S_q, S_r, and S_d are the selectivities of the radiative emission reactions, quenching reactions, NO_x conversion reactions, and CO dissociation, respectively; R_i is the reaction rate of reaction type i; k_I, k_q, k_r, and k_d are the rate constants of radiation, quenching, NO_x conversion, and CO dissociation, respectively; and C is the initial mole concentration of the subscripted species.

This type of selectivity analysis is an effective method to examine the significance of the active species. Only the active species that significantly contribute to the formation and conversion of NO_x and CO need to be considered. In this work, the highest initial NO concentration with or without CO is about 600 ppm, while the highest CO concentration is 1.01 mol % in balance Ar. Without CO, at 141 kPa and 300 K, the concentrations of 600 ppm NO and balance Ar are 3.38×10^{-8} and 5.64×10^{-5} mol cm^{-3}, respectively. Table II shows the results of this selectivity analysis, performed by substituting these concentrations and the rate constants for the consumption of active species by radiation, quenching, and NO_x conversion (listed in Table II) into Eqs. (5a)–(5c) to yield the selectivities for the three parallel processes. Table II does not include a column for selectivities of CO dissociation because it is zero by definition for these conditions without CO.

For the four excited states of Ar with $3p^5\,4s$ configurations, quenching reactions with Ar include two-body quenching reactions and three-body association reactions[10] as follows:

$$\mathrm{Ar}(4s) + \mathrm{Ar} \rightarrow \mathrm{Ar} + \mathrm{Ar}, \quad R_{q2} = k_{q2} \cdot C_{\mathrm{Ar}(4s)} \cdot C_{\mathrm{Ar}} \tag{6}$$

$$\mathrm{Ar}(4s) + \mathrm{Ar} + \mathrm{Ar} \rightarrow \mathrm{Ar_2}^{*} + \mathrm{Ar}, \quad R_{q3} = k_{q3} \cdot C_{\mathrm{Ar}(4s)} \cdot {C_{\mathrm{Ar}}}^2 \tag{7}$$

where Ar($4s$) represents any of the four Ar $3p^5\,4s$ excited states; Ar_2^* are the excited states of Ar_2 molecules; R_{q2} and R_{q3} are reaction rates of (6) and (7), respectively; and k_{q2} and k_{q3} are quenching rate constants of the two-body reaction (6) and the three-body reaction (7), respectively. The value of $k_q C_{Ar}$ listed in the third column of Table II is the sum of these two quenching rates as follows:

$$k_q C_{\mathrm{Ar}} = k_{q2} \cdot C_{\mathrm{Ar}} + k_{q3} \cdot {C_{\mathrm{Ar}}}^2. \tag{8}$$

Of the four excited states of Ar with $3p^5\,4s$ configurations, Ar($^3P_1$) and Ar($^1P_1$) predominantly contribute to natural radiation to the ground state because of their very short natural radiation lifetimes (<9.5 ns).[10] For Ar($^3P_2$), rate constants of the two-body and three-body reactions are 1.26×10^{9} cm^3 mol^{-1} s^{-1} and 2.17×10^{15} cm^6 mol^{-2} s^{-1},[10] respectively. As a result, the net reaction rate of the three-body association reactions is about two orders of magnitude higher than that of the two-body quenching reactions. This indicates that S_q of Ar($^3P_2$) in Table II represents the selectivity of the three-body association reaction. The product of this reaction of Ar($^3P_2$) is $Ar_2(^3\Sigma_u^+)$, which has a relatively long natural radiation lifetime of 3.15 μs,[25] an excitation energy of 10.6 eV,[25] and reacts with all NO_x species, as found by Mehnert *et al.*[26] and Oka *et al.*[27] Therefore, the net yield of Ar($^3P_2$), including $Ar_2(^3\Sigma_u^+)$, that contributes to NO_x conversion is nearly 100%, which indicates that Ar($^3P_2$) is an important active species species for NO_x conversion. For Ar($^3P_0$), the rate constants of the two-body and the three-body reactions are 3.19×10^{9} cm^3 mol^{-2} s^{-1} and 3.01×10^{15} cm^6 mol^{-2} s^{-1},[10] respectively. Therefore, the net reaction rate of the three-body association reaction is about 50 times higher than that of the two-body quenching reaction, which is again negligible. The product of the three-body re-

TABLE III. Initial selectivity of active species consumption in nonthermal argon plasma with 1.01% CO by radiation, quenching, NO conversion, and CO dissociation.

Ar excited states	K_I[a] (s^{-1})	k_qC_{Ar}[b] (s^{-1})	$k_rC_{NO_x}$[c] (s^{-1})	k_dC_{CO}[c] (s^{-1})	S_I (%)	$S_{q,Ar}$ (%)	S_{r,NO_x} (%)	$S_{d,CO}$ (%)
$^3P_2$	2.63×10^{-2}	6.97×10^6	4.47×10^6	4.75×10^6	~0	43.1	27.6	29.3
$^3P_1$	1.05×10^8	9.44×10^6	6.53×10^6	1.76×10^7	75.8	6.8	4.7	12.7
$^3P_0$	2.23×10^{-2}	9.75×10^6	5.11×10^6	4.41×10^7	~0	16.5	8.7	74.8
$^1P_1$	4.00×10^8	4.73×10^6	1.10×10^7	2.89×10^7	90.0	1.1	2.5	6.5
$2p_{10}$	2.47×10^7	6.79×10^8	⋯	⋯	3.5	96.5	⋯	⋯
$2p_9$	3.26×10^7	1.09×10^9	9.38×10^6	1.70×10^8	2.6	83.7	0.7	13.0
$2p_8$	3.27×10^7	1.09×10^9	9.38×10^6	1.70×10^8	2.6	83.7	0.7	13.0
$2p_7$	3.31×10^7	2.61×10^9	⋯	⋯	1.3	98.7	⋯	⋯
$2p_6$	3.40×10^7	1.22×10^9	1.02×10^7	8.49×10^7	2.5	90.4	0.8	6.3
$2p_5$	4.10×10^7	1.60×10^9	1.02×10^7	9.17×10^7	2.4	91.8	0.6	5.3
$2p_4$	3.41×10^7	1.19×10^9	⋯	⋯	2.8	97.2	⋯	⋯
$2p_3$	3.45×10^7	1.05×10^9	⋯	⋯	3.2	96.8	⋯	⋯
$2p_2$	3.53×10^7	6.45×10^8	⋯	⋯	5.2	94.8	⋯	⋯
$2p_1$	4.61×10^7	1.36×10^9	1.59×10^7	3.73×10^7	3.2	93.2	1.1	2.6

[a]References 34–38.
[b]References 19–22.
[c]References 39 and 40.

action of $Ar(^3P_0)$, $Ar_2(^1\Sigma_u^+)$, has a short natural radiation lifetime of 4 ns (Ref. 25) and hence it predominantly relaxes to the ground state without contributing appreciably to NO_x reactions. The net yield of $Ar(^3P_0)$ contributing to NO_x conversion is 34.4%, as shown in Table II.

Of the ten excited states of Ar with $3p^5\,4p$ configurations, $Ar(2p_1)$, $Ar(2p_5)$, $Ar(2p_6)$, $Ar(2p_8)$, and $Ar(2p_9)$ are predominantly quenched by Ar. Although there are no reports of the reaction rate constants of NO_x with $Ar(2p_2)$, $Ar(2p_3)$, $Ar(2p_4)$, $Ar(2p_7)$, and $Ar(2p_{10})$, these rate constants are assumed to be similar to the reported values for the other five states (listed in Table II) because of their similar excitation energies.[10] Therefore, the ten $3p^5\,4p$ Ar configurations probably do not contribute to NO_x conversion; the five reported values of S_{r,NO_x} are all less than ~1%. These results suggest that the Ar excited states, except for $Ar(^3P_2)$ and $Ar(^3P_0)$, do not contribute to NO_x conversion. They are predominantly quenched by Ar and CO, or emit natural radiation, if they are formed in the nonthermal plasma.

With 1.01% CO, at 141 kPa and 300 K, the concentrations of 600 ppm NO, 1.01% CO, and balance Ar are 3.38×10^{-8}, 5.70×10^{-7}, and 5.58×10^{-5} mol cm^{-3}, respectively. Table III shows the selectivities of consumption of the 14 excited states of Ar by the four parallel processes of radiation, quenching, NO_x conversion, and CO dissociation [Eqs. (5a)–(5d)] obtained by an analysis similar to that used to develop Table II. With 1.01% CO, none of the electronic excited states of Ar, except $Ar(^3P_2)$ and $Ar(^3P_0)$, exceeds 13% selectivity for CO dissociation (Table III). At lower (ppm) CO concentrations, none of the Ar excited states contribute significantly to CO dissociation.

This analysis indicates that only two Ar excited states, $Ar(^3P_2)$ and $Ar(^3P_0)$, contribute to NO_x conversion and CO dissociation. However, previous investigations[20,21,28–32] have shown that the yield of $Ar(^3P_0)$ produced by the electron collision reaction is 10%–15% of the yield of $Ar(^3P_2)$. Moreover, without CO, virtually all $Ar(^3P_2)$ contribute to NO_x conversion, compared to only about 1/3 of $Ar(^3P_0)$, as discussed in the context of Table II. The lower $Ar(^3P_0)$ concentration and the smaller $Ar(^3P_0)$ contribution to NO_x conversion justify the use of the reaction rate constant for $Ar(^3P_2)$ alone without a serious error, given the similarity of the $Ar(^3P_2)$ and $Ar(^3P_0)$ reactions. This result suggests that a single electron collision reaction,

$$e + Ar \rightarrow Ar(^3P_2) + e, \tag{9'}$$

may be used to model all NO_x reactions in Ar and in NO_x plus CO in Ar. This conjecture is confirmed by the following modeling investigation.

C. Mechanism and kinetics

Numerous series and parallel reactions among active species and stable species are possible following the electron collision reactions. Without CO, a total of 43 reactions [(9)–(51) shown in Table IV] are selected to simulate NO_x concentration, based on a rough selectivity analysis to determine the controlling reactions, assuming that the slowest reaction among series reactions is the controlling step, whereas the fastest reaction among parallel reactions is the controlling step. These 43 reactions involved in NO_x conversion are used to analyze the NO/Ar and N_2O/Ar reaction systems.

A previously developed lumped kinetic model[6] is used to describe the concentrations of all species as a function of power input. The important model parameters embodying the rate of electron collision reactions are α and β, as shown in the following equation:

$$k[e] = \beta\sqrt{\frac{1}{\alpha P}}W^{0.75}\exp\left(-\frac{\alpha P}{W}\right), \tag{10'}$$

where k is the rate constant of the electron collision reaction (with units of $cm^3\ mol^{-1}\ s^{-1}$), $[e]$ is the electron concentration (mol cm^{-3}), P is the system pressure (atm), and W is the power input (J s^{-1}). This expression, based on a Maxwellian

TABLE IV. Reactions and rate constants for NO_x and CO in nonthermal Ar plasma.

Chemical reaction	Rate constant ($cm^3\ mol^{-1}\ s^{-1}$)	Source	Equation
$e+Ar \rightarrow Ar(^3P_2)+e$	$k_5=\frac{\beta}{[e]}\sqrt{\frac{1}{\alpha P}}W^{0.75}\exp\left(-\frac{\alpha P}{W}\right)$	This work	(9)
$Ar(^3P_2)+NO \rightarrow Ar+N+O$	1.44×10^{14}	Ref. 40	(10)
$Ar(^3P_2)+NO_2 \rightarrow Ar+NO+O$	3.91×10^{14}	Ref. 40	(11)
$Ar(^3P_2)+N_2O \rightarrow Ar+N_2(B)+O$	2.65×10^{14}	Ref. 41	(12)
$Ar(^3P_2)+O_2 \rightarrow Ar+O+O$	1.32×10^{14}	Ref. 40	(13)
$Ar(^3P_2)+N_2 \rightarrow Ar+N_2(C)$	2.17×10^{13}	Ref. 39	(14)
$Ar(^3P_2)+Ar \rightarrow Ar+Ar$	1.30×10^{9}	Ref. 21	(15)
$Ar(^3P_2)+2Ar \rightarrow Ar_2(^3\Sigma_u^+)+Ar$	2.17×10^{15}[Ar]	Ref. 42	(16)
$Ar_2(^3\Sigma_u^+) \rightarrow Ar+Ar+h\nu$	3.17×10^{5}	Ref. 25	(17)
$Ar_2(^3\Sigma_u^+)+Ar \rightarrow Ar+Ar+Ar$	6.02×10^{9}	Ref. 26	(18)
$Ar_2(^3\Sigma_u^+)+NO \rightarrow 2Ar+N+O$	1.87×10^{14}	Ref. 27	(19)
$Ar_2(^3\Sigma_u^+)+NO_2 \rightarrow 2Ar+NO+O$	5.08×10^{14}	Estimated	(20)
$Ar_2(^3\Sigma_u^+)+N_2O \rightarrow 2Ar+N_2+O$	3.31×10^{14}	Ref. 27	(21)
$Ar_2(^3\Sigma_u^+)+N_2 \rightarrow 2Ar+N_2(B)$	7.22×10^{12}	Ref. 26	(22)
$Ar_2(^3\Sigma_u^+)+O_2 \rightarrow 2Ar+O+O$	1.57×10^{14}	Ref. 27	(23)
$N+NO \rightarrow N_2+O$	1.87×10^{13}	Ref. 43	(24)
$N+NO_2 \rightarrow N_2O+O$	1.81×10^{12}	Ref. 43	(25)
$N+NO_2 \rightarrow N_2+O_2$	4.21×10^{11}	Ref. 44	(26)
$N+NO_2 \rightarrow N_2+2O$	5.48×10^{11}	Ref. 44	(27)
$N+NO_2 \rightarrow 2NO$	1.38×10^{12}	Ref. 44	(28)
$N+N+Ar \rightarrow N_2+Ar$	1.59×10^{15}[Ar]	Ref. 45	(29)
$N+O+Ar \rightarrow NO+Ar$	3.77×10^{15}[Ar]	Ref. 45	(30)
$O+NO+Ar \rightarrow NO_2+Ar$	$k_0=2.43\times10^{16}$[Ar] $k_\infty=1.81\times10^{13}$ $Fc=0.85$	Refs. 46 and 47	(31)
$O+NO_2+Ar \rightarrow NO_3+Ar$	$k_0=3.26\times10^{16}$[Ar] $k_\infty=1.32\times10^{13}$ $Fc=0.80$	Ref. 47	(32)
$O+NO_2 \rightarrow NO+O_2$	5.85×10^{12}	Ref. 47	(33)
$O+NO_3 \rightarrow NO_2+O_2$	1.02×10^{13}	Ref. 47	(34)
$O+O+Ar \rightarrow O_2+Ar$	3.79×10^{14}[Ar]	Ref. 48	(35)
$N_2(A)+NO \rightarrow N_2+NO$	3.85×10^{13}	Ref. 49	(36)
$N_2(A)+NO_2 \rightarrow N_2+NO+O$	7.83×10^{12}	Ref. 49	(37)
$N_2(A)+N_2O \rightarrow N_2+N_2+O$	3.73×10^{12}	Ref. 49	(38)
$N_2(A)+O_2 \rightarrow N_2+2O$	1.51×10^{12}	Ref. 50	(39)
$N_2(A)+O_2 \rightarrow N_2O+O$	4.70×10^{10}	Ref. 44	(40)
$N_2(A)+O_2 \rightarrow N_2+O_2$	7.77×10^{11}	Ref. 44	(41)
$N_2(C) \rightarrow N_2(B)+h\nu$	2.73×10^{7}	Ref. 51	(42)
$N_2(C)+Ar \rightarrow N_2(B)+Ar$	8.19×10^{11}	Ref. 52	(43)
$N_2(B) \rightarrow N_2(A)+h\nu$	2.00×10^{5}	Ref. 53	(44)
$N_2(B)+NO \rightarrow N_2(A)+NO$	1.44×10^{14}	Ref. 44	(45)
$N_2(B)+N_2O \rightarrow N_2+N_2+O$	9.63×10^{13}	Ref. 54	(46)
$N_2(B)+O_2 \rightarrow N_2+O+O$	1.81×10^{14}	Ref. 44	(47)
$N_2(B)+N_2 \rightarrow N_2(A)+N_2$	1.81×10^{13}	Ref. 55	(48)
$N_2(B)+Ar \rightarrow N_2(A)+Ar$	9.63×10^{11}	Ref. 56	(49)
$NO+NO_3 \rightarrow 2NO_2$	1.57×10^{13}	Ref. 47	(50)
$2NO+O_2 \rightarrow 2NO_2$	7.25×10^{9}	Ref. 47	(51)
$CO+Ar(^3P_2) \rightarrow Ar+C+O$	1.62×10^{13}	Ref. 24	(52)
$CO+Ar_2(^3\Sigma_u^+) \rightarrow 2Ar+CO$	9.63×10^{13}	Ref. 27	(53)
$CO+N_2(A) \rightarrow N_2+CO$	9.63×10^{11}	Ref. 49	(54)
$CO+N_2(B) \rightarrow N_2(A)+CO$	5.12×10^{13}	Ref. 54	(55)
$CO+N_2(C) \rightarrow N_2(B)+CO$	1.44×10^{14}	Ref. 57	(56)
$CO+O+Ar \rightarrow CO_2+Ar$	6.61×10^{11}[Ar]	Ref. 58	(57)
$CO_2+Ar(^3P_2) \rightarrow Ar+CO+O$	3.37×10^{14}	Ref. 59	(58)
$CO_2+Ar_2(^3\Sigma_u^+) \rightarrow 2Ar+CO+O$	4.09×10^{14}	Ref. 27	(59)

TABLE IV. (*Continued.*)

Chemical reaction	Rate constant ($cm^3\ mol^{-1}\ s^{-1}$)	Source	Equation
$CO_2+N_2(A)\rightarrow N_2+CO+O$	1.20×10^{10}	Ref. 49	(60)
$CO_2+N_2(B)\rightarrow N_2+CO+O$	1.20×10^{14}	Ref. 55	(61)
$CO_2+N_2(C)\rightarrow N_2+CO+O$	2.33×10^{14}	Ref. 60	(62)
$C+NO\rightarrow CN+O$	3.35×10^{13}	Ref. 61	(63)
$C+NO\rightarrow N+CO$	2.10×10^{13}	Ref. 61	(64)
$C+N_2O\rightarrow CN+NO$	5.12×10^{12}	Ref. 62	(65)
$C+O_2\rightarrow CO+O$	2.83×10^{13}	Ref. 63	(66)
$C+CO\rightarrow C_2O$	7.83×10^{10}	Ref. 62	(67)
$C_2O+NO\rightarrow NCO+CO$	2.81×10^{13}	Ref. 64	(68)
$C_2O+NO\rightarrow CN+CO_2$	4.20×10^{12}	Ref. 64	(69)
$C_2O+NO_2\rightarrow NCO+CO_2$	4.15×10^{13}	Ref. 64	(70)
$C_2O+O_2\rightarrow CO+CO+O$	2.44×10^{11}	Ref. 65	(71)
$C_2O+O\rightarrow CO+CO$	3.01×10^{13}	Ref. 58	(72)
$C_2O+N\rightarrow CN+CO$	3.31×10^{14}	Ref. 66	(73)
$CN+NO\rightarrow N_2+CO$	2.23×10^{13}	Ref. 67	(74)
$CN+NO_2\rightarrow NCO+NO$	4.85×10^{13}	Ref. 68	(75)
$CN+NO_2\rightarrow CO+N_2O$	4.27×10^{12}	Ref. 68	(76)
$CN+NO_2\rightarrow CO_2+N_2$	3.13×10^{12}	Ref. 68	(77)
$CN+O_2\rightarrow NCO+O$	1.16×10^{13}	Ref. 69	(78)
$CN+O_2\rightarrow CO+NO$	3.46×10^{12}	Ref. 69	(79)
$CN+O\rightarrow N+CO$	8.74×10^{13}	Ref. 61	(80)
$CN+N\rightarrow N_2+C$	6.02×10^{13}	Ref. 70	(81)
$NCO+NO\rightarrow CO+N_2O$	8.73×10^{12}	Ref. 69	(82)
$NCO+NO\rightarrow CO_2+N_2$	1.11×10^{13}	Ref. 69	(83)
$NCO+NO_2\rightarrow NO+NO+CO$	9.05×10^{11}	Ref. 68	(84)
$NCO+NO_2\rightarrow N_2O+CO_2$	1.00×10^{13}	Ref. 68	(85)
$NCO+O_2\rightarrow NO_2+CO$	3.01×10^{9}	Ref. 69	(86)
$NCO+O\rightarrow NO+CO$	1.99×10^{13}	Ref. 69	(87)
$NCO+NCO\rightarrow N_2+CO+CO$	1.81×10^{13}	Ref. 71	(88)
$NCO+N\rightarrow N_2+CO$	3.31×10^{13}	Ref. 72	(89)

distribution function for the electron velocity, semiempirically describes the rate of electron collision reactions through a pseudo-first-order rate constant by combining the true rate constant with the electron concentration.[33] The parameters α and β are determined from experimental data using a previously presented optimization method.[6] This means that two model parameters are needed to describe the single important electron collision reaction with Ar (9). There are 14 components [Ar, $Ar(^3P_2)$, $Ar_2(^3\Sigma_u^+)$, NO, NO_2, NO_3, N_2O, N_2, O_2, N, O, $N_2(A)$, $N_2(B)$, and $N_2(C)$] in this reaction system, as shown in Table IV. Therefore, there are 14 equations for each of the seven power inputs, which leads to a total of 98 equations used to determine the two parameters (α and β) for 314 ppm NO in Ar at 3.45×10^{-4} $m^3\ s^{-1}$ and 141 kPa using the previously reported optimization method.[6] The concentrations of N_2 and O_2 at the outlet of the reactor are obtained using the material balance of nitrogen and oxygen. The values of α_1 and β_1 for

$$e + \mathrm{Ar} \rightarrow \mathrm{Ar}(^3P_2) + e \qquad (9'')$$

are found to be 4.90 $J^{-0.25}\ s^{-0.75}$ and 1.63×10^{-5} J $atm^{-1}\ s^{-1}$, respectively.

Figure 3(a) shows the measured and correlated NO, NO_2, and N_2O concentrations for the experiment used in fitting α_1 and β_1. The correlated curves in Fig. 3(a) reasonably represent the experimental data because these data have been used for fitting. The same α_1 and β_1 values are used without further fitting to predict the concentrations obtained at two other experimental conditions: 414 ppm NO in Ar and 570 ppm NO in Ar [Figs. 3(b) and 3(c)]. All predicted data match the experimental data (except for the experimental

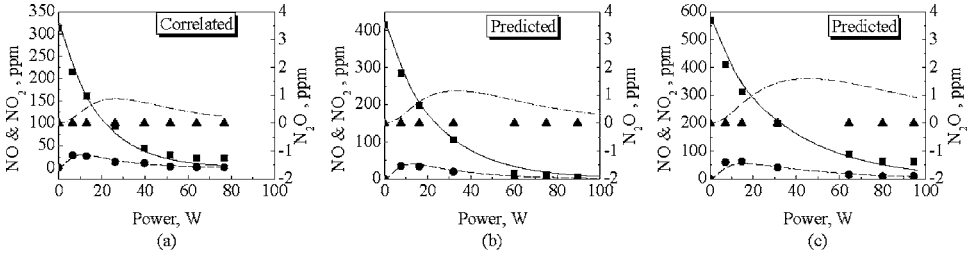

FIG. 3. Comparison of experimental data and calculated data for the conversion of NO in Ar at a flow rate of 3.45×10^{-4} $m^3\ s^{-1}$ and 141 kPa: (a) 314 ppm NO in Ar, (b) 414 ppm NO in Ar, and (c) 570 ppm NO in Ar. Experimental data: (■) NO, (●) NO_2, and (▲) N_2O; calculated data: (—) NO, (---), NO_2, and (---) N_2O.

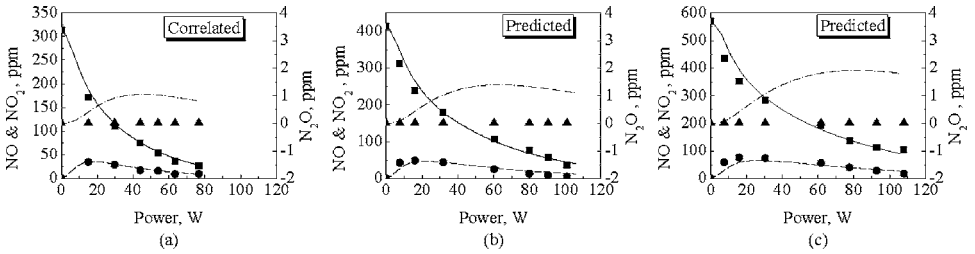

FIG. 4. Comparison of experimental data and calculated data for the conversion of NO in Ar at a flow rate of 4.01×10^{-4} m^3 s^{-1} and 189 kPa: (a) 314 ppm NO in Ar, (b) 414 ppm NO in Ar, and (c) 570 ppm NO in Ar. Experimental data: (■) NO, (●) NO_2, and (▲) N_2O; calculated data: (—) NO, (---) NO_2, and (···) N_2O.

N_2O concentrations that are reported as 0 because they are below the experimental detection limit of 5 ppm). This confirms that a single set of α_1 and β_1 values derived from a single set of experimental data can predict the PCDR product compositions obtained at other gas inlet concentrations using the set of 43 reactions shown in Table IV. Previous investigations[9,14,15] have shown that the lumped model accurately describes power input and gas residence time effects as well as inlet concentration.

A previous investigation[14] also showed that gas pressure affects the rate of electron collision reactions. At 189 kPa, for $e+\mathrm{Ar}\rightarrow\mathrm{Ar}(^3P_2)+e$ (9) at 314 ppm NO in Ar at 4.01×10^{-4} m^3 s^{-1}, the model parameters α_2 and β_2 are found to be 4.60 J$^{-0.25}$ s$^{-0.75}$ and 1.32×10^{-5} J atm^{-1} s^{-1}, respectively.

The same α_2 and β_2 values are used without further fitting to predict the concentrations obtained at 414 and 570 ppm NO in Ar. Figures 4(a)–4(c) show that all correlated and predicted data match the measured experimental data, which further confirms the reaction mechanism involving 43 reactions for NO conversion in Ar. Comparison of the model parameters obtained for reaction (9) at 141 and 189 kPa shows that the α parameters are approximately the same for both pressures, while β_2 at 189 kPa is lower than β_1 at 141 kPa. This is consistent with our previous results[14] that showed β decreases with increasing pressure.

Again, N_2O is not detected by FTIR for NO conversion in Ar. All calculated data in Figs. 3 and 4 show that the N_2O concentration at the outlet of the PCDR is less than 2 ppm, which is consistent with the experimental observation of N_2O concentrations below the 5 ppm FTIR detection limit.

In our previous work,[11] we used Ar^+ as the only active species that contributes to NO or N_2O conversion in Ar. As a result, that work required two different sets of α and β parameters for electron collision reactions to predict NO and N_2O conversions, which implied that the rate of electron collision reactions with Ar to form Ar^+ is different for NO in Ar compared to N_2O in Ar. That result is difficult to rationalize and suggests that Ar^+ may not actually be involved.

In the present study, therefore, we drop the hypothesis that Ar^+ species are involved and instead assume that $\mathrm{Ar}(^3P_2)$ is the only active species involved. As a result, the model using the same parameters for NO conversion in Ar (α_1 and β_1, and α_2 and β_2, determined at 141 and 189 kPa, respectively) also accurately predicts the observed N_2O concentrations in Ar, as shown in Figs. 5(a) and 5(b). The accurate estimate of both the NO and N_2O experimental data using the same model parameters on the basis of $\mathrm{Ar}(^3P_2)$ alone confirms that the true active species contributing to NO_x conversion are the excited neutral states of Ar, and hence, that the contribution of Ar^+ is negligible.

With CO, the reaction mechanism is more complex because of the dissociation of CO by $\mathrm{Ar}(^3P_2)$ to form atomic C,[24] which leads to the formation of radicals, such as CN, C_2O, and NCO. These radicals can also react with NO_x. Therefore, with CO present, 38 additional reactions [(52)–(89) in Table IV] are selected through a similar selectivity analysis to form a model with a total of 81 reactions for the NO/CO/Ar and N_2O/CO/Ar reaction systems.

For low (ppm) concentrations of CO at 3.45×10^{-4} m^3 s^{-1} and 141 kPa, Fig. 6 shows the predicted data

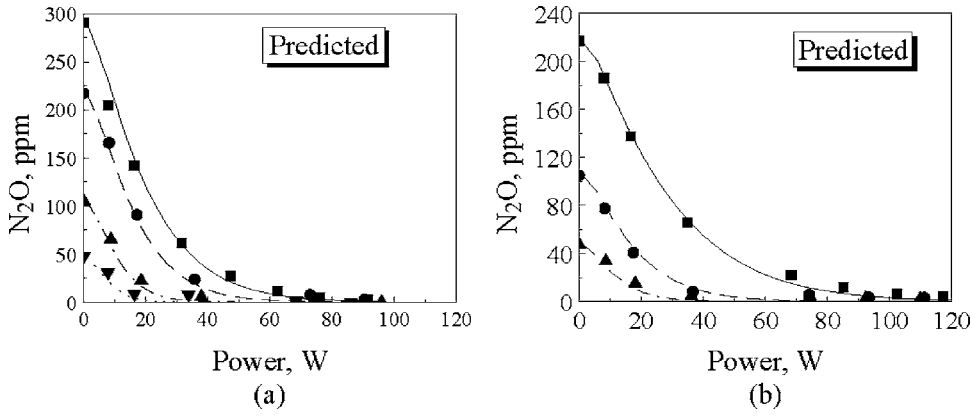

FIG. 5. Comparison of experimental data and predicted data for the conversion of N_2O in Ar (a) at a flow rate of 3.45×10^{-4} m^3 s^{-1} and 141 kPa. Experimental data: (■) 290 ppm N_2O in Ar, (●) 217 ppm N_2O in Ar, (▲) 103 ppm N_2O in Ar, and (▼) 47.6 ppm N_2O in Ar; calculated data: (—) 290 ppm N_2O in Ar, (---) 217 ppm N_2O in Ar, (··-··) 103 ppm N_2O in Ar, and (···) 47.6 ppm N_2O in Ar; and (b) at a flow rate of 4.01×10^{-4} m^3 s^{-1} and 189 kPa. Experimental data: (■) 217 ppm N_2O in Ar, (●) 103 ppm N_2O in Ar, and (▲) 47.6 ppm N_2O in Ar; calculated data: (—) 217 ppm N_2O in Ar, (---) 103 ppm N_2O in Ar, and (··-··) 47.6 ppm N_2O in Ar.

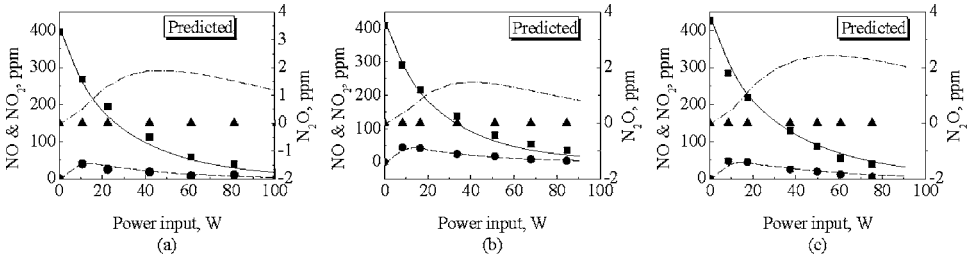

FIG. 6. Comparison of experimental data and predicted data for NO conversion in Ar with low (ppm) CO concentrations at a flow rate of 3.45×10^{-4} m^3 s^{-1} and 141 kPa: (a) 396 ppm NO+435 ppm CO in Ar, (b) 411 ppm NO+203 ppm CO in Ar, and (c) 426 ppm NO+619 ppm CO in Ar. Experimental data: (■) NO, (●) NO_2, and (▲) N_2O; calculated data: (—) NO, (---) NO_2, and (--) N_2O.

using model parameters α_1 and β_1 determined for NO conversion in Ar in the absence of CO at 141 kPa and the experimentally measured NO, NO_2, and N_2O concentrations as a function of power input. Figure 6(a) is for 396 ppm NO plus 435 ppm CO in Ar, Fig. 6(b) is for 411 ppm NO plus 203 ppm CO in Ar, and Fig. 6(c) is for 426 ppm NO plus 619 ppm CO in Ar. The calculated results are found to be consistent with the experimental results, including N_2O, which remains below the experimental detection limit.

Figure 7(a) compares the predicted and the measured concentrations of NO, NO_2, and N_2O as a function of power input for 1.01% CO concentrations with 575 ppm NO in Ar at 3.45×10^{-4} m^3 s^{-1} and 141 kPa. The same model parameters (α_1 and β_1) determined for NO conversion in Ar without CO at 141 kPa are used to calculate the concentrations of NO, NO_2, and N_2O in Fig. 7(a). Figures 7(b) and 7(c) compare the predicted and measured concentrations of NO, NO_2, and N_2O as a function of power input at 4.01×10^{-4} m^3 s^{-1} and 189 kPa for 1.01% CO with 440 and 577 ppm NO in Ar, respectively. The same model parameters (α_2 and β_2) determined for NO conversion in Ar without CO at 189 kPa are used to calculate the concentrations of NO, NO_2, and N_2O in Figs. 7(b) and 7(c). The results of Fig. 7 show that all experimental data can be predicted using the same reaction mechanism (81 reactions shown in Table IV) and a single electron collision reaction (9), even at higher concentrations (such as 1.01%) of CO. This result supports our conjecture that electron collision reactions with CO at high CO concentrations are not significant because the active CO species are quenched by Ar or CO.

Figures 8(a)–8(c) compare the predicted and measured N_2O concentrations as a function of power input at low (ppm) CO concentrations in various N_2O concentrations in Ar at 3.45×10^{-4} m^3 s^{-1} and 141 kPa using the α_1 and β_1 determined for NO conversion in Ar at 141 kPa. Figure 9 compares the predicted and measured N_2O concentrations as a function of power input with high (1.01%) CO concentrations in several N_2O concentrations in Ar at 4.01×10^{-4} m^3 s^{-1} and 189 kPa using the α_2 and β_2 determined for NO conversion in Ar at 189 kPa. All N_2O concentrations with CO present are predicted, which further confirms the 81 reaction mechanism shown in Table IV.

The results in Figs. 3–9 demonstrate two points: (1) a single electron collision reaction (9) for $Ar(^3P_2)$ can predict NO, NO_2, and N_2O concentrations without and with CO and (2) at a given pressure, the same model parameters α and β can be used to predict NO, NO_2, and N_2O concentrations without and with CO. These results cannot be obtained with Ar^+ as the active species responsible for plasma reactions, as demonstrated recently.[11]

D. Effect of CO on NO and N_2O conversions

The model prediction results shown in Figs. 6–9 suggest that the mechanism of NO or N_2O conversion with CO in Ar plasma (shown in Table IV), combined with the lumped model parameters (α_1 and β_1 at 141 kPa or α_2 and β_2 at 189 kPa), captures the effect of CO on NO_x concentrations. Therefore, this reaction mechanism and this kinetic model are used to investigate the effect of CO concentration on NO or N_2O conversion in Ar plasma.

An example is shown in Fig. 10. The calculation is conducted for an inlet concentration of 600 ppm NO in Ar with variable CO concentration, from 0 to 12 000 ppm (mole fraction of 1.2%), at 4.01×10^{-4} m^3 s^{-1}, 189 kPa, and a constant power input of 60 W, using model parameters α_2 and β_2. Similar results were obtained for other conditions. Figure 10(a) shows the NO, NO_2, and N_2O concentrations as a

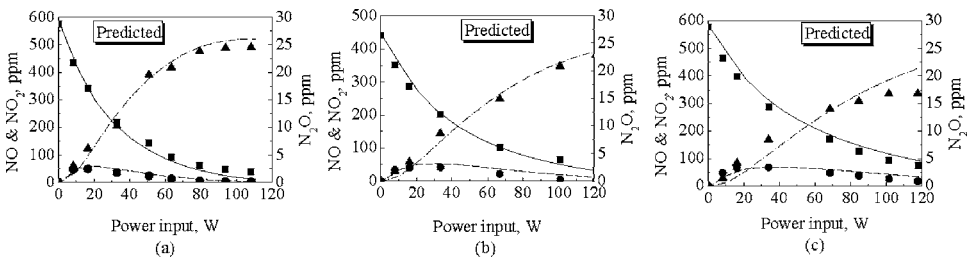

FIG. 7. Comparison of experimental data and predicted data for NO conversion in Ar with 1.01% CO concentrations: (a) 575 ppm NO+1.01% CO in Ar at a flow rate of 3.45×10^{-4} m^3 s^{-1} and 141 kPa, (b) 440 ppm NO+1.01% CO in Ar, and (c) 577 ppm NO+1.01% CO in Ar at a flow rate of 4.01×10^{-4} m^3 s^{-1} and 189 kPa. Experimental data: (■) NO, (●) NO_2, and (▲) N_2O; calculated data: (—) NO, (---) NO_2, and (--) N_2O.

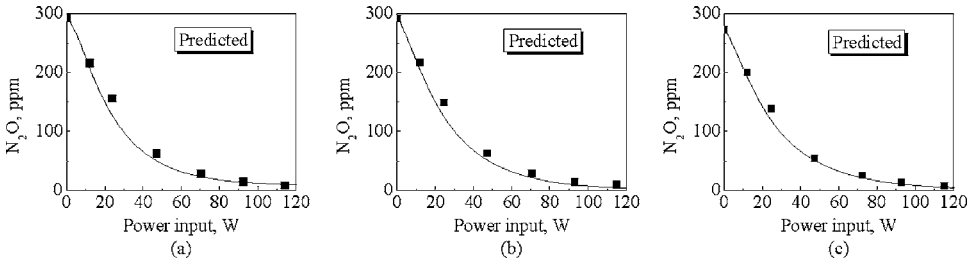

FIG. 8. Comparison of experimental data and predicted data for N_2O conversion in Ar with low (ppm) CO concentrations at a flow rate of 3.45×10^{-4} m^3 s^{-1} and 141 kPa: (a) 293 ppm N_2O+197 ppm CO in Ar, (b) 292 ppm N_2O+305 ppm CO in Ar, and (c) 273 ppm N_2O+389 ppm CO in Ar. Experimental data: (■) N_2O; calculated data: (—) N_2O.

function of CO concentration. With increasing CO concentration, NO concentration initially increases, reaches a maximum at around 2400 ppm CO, and then decreases. NO_2 concentration follows a similar trend, but the range of NO_2 variation is only around 12 ppm. N_2O concentration linearly increases with increasing CO concentration. At CO concentrations less than 3200 ppm, the predicted N_2O concentrations are below the experimental detection limit of 5 ppm, which is consistent with the observed experimental results [Figs. 1(a), 3, 4, and 6].

The variation of NO and NO_2 concentrations with increasing CO concentration indicates that NO conversion initially decreases, reaches a minimum, and then increases with increasing CO concentration, as shown in Fig. 10(b). NO conversion decreases sharply with increasing CO concentration from 0 to 2400 ppm, while NO conversion increases slowly with increasing CO concentration from 2400 to 12 000 ppm. When CO concentration is about 1.01% (10 100 ppm), concentrations of NO and NO_2 [Fig. 10(a)] and NO conversions [Fig. 10(b)] are approximately the same as those without CO. The results in Fig. 10 emulate the experimental observations that CO concentrations of 200–600 ppm inhibit NO conversion and N_2O is not detectable [Figs. 1(a) and 1(b)], whereas 1.01% CO has no effect on NO conversion, but N_2O is detected [Figs. 1(c) and 1(d)].

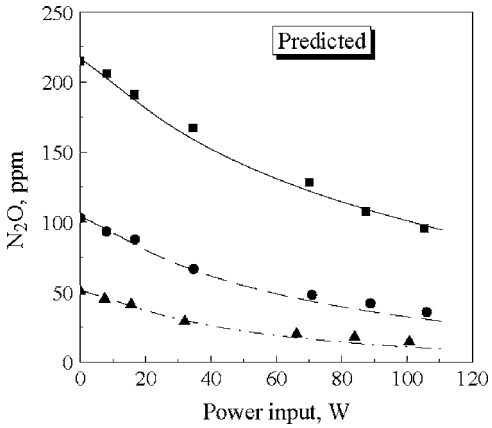

FIG. 9. Comparison of experimental data and predicted data for N_2O conversion in Ar with 1.01% CO at a flow rate of 4.01×10^{-4} m^3 s^{-1} and 189 kPa. Experimental data: (■) 215 ppm N_2O plus 1.01% CO in Ar, (●) 103 ppm N_2O plus 1.01% CO in Ar, and (▲) 50.7 ppm N_2O plus 1.01% CO in Ar; calculated data: (—) 215 ppm N_2O plus 1.01% CO in Ar, (---) 103 ppm N_2O plus 1.01% CO in Ar, and (···) 50.7 ppm N_2O plus 1.01% CO in Ar.

The results presented in Fig. 10 can be explained by the reaction mechanism shown in Table IV. During electrical discharge in the PCDR, the active species $Ar(^3P_2)$ is produced, which initiates the subsequent chemical reactions between the pulses. $Ar(^3P_2)$ mainly contributes to NO dissociation in (10), formation of the excited state $Ar_2(^3\Sigma_u^+)$ in (16), and CO dissociation in (52) as follow:

$$Ar(^3P_2) + NO \rightarrow Ar + N + O,$$

$$k = 1.44 \times 10^{14}\ cm^3\ mol^{-1}\ s^{-1} \qquad (10'')$$

$$Ar(^3P_2) + 2Ar \rightarrow Ar_2(^3\Sigma_u^+) + Ar,$$

$$k = 2.17 \times 10^{15}\ cm^6\ mol^{-2}\ s^{-1} \qquad (16')$$

$$Ar(^3P_2) + CO \rightarrow Ar + C + O,$$

$$k = 1.62 \times 10^{13}\ cm^3\ mol^{-1}\ s^{-1}. \qquad (52')$$

$Ar_2(^3\Sigma_u^+)$ further contributes to NO dissociation in (19) and quenching with CO in (53) as follow:

$$Ar_2(^3\Sigma_u^+) + NO \rightarrow 2Ar + N + O,$$

$$k = 1.87 \times 10^{14}\ cm^3\ mol^{-1}\ s^{-1} \qquad (19')$$

$$Ar_2(^3\Sigma_u^+) + CO \rightarrow 2Ar + CO,$$

$$k = 9.63 \times 10^{13}\ cm^3\ mol^{-1}\ s^{-1}. \qquad (53')$$

At low CO concentrations ($< \sim 2400$ ppm), the selectivity of $Ar(^3P_2)$ to NO dissociation (S_{r,NO_x}) by (10) is low (39.1% without CO, as shown in Table II) and decreases with increasing CO concentration (ultimately becoming 27.6% at 1.01% CO, Table III). The $Ar(^3P_2)$ selectivity to CO dissociation ($S_{d,CO}$) by (52) is low because the CO concentration is low and the rate constant of (52) is about one order of magnitude lower than that of (10). Therefore, most $Ar(^3P_2)$ (60.9% at zero CO concentration, Table II) forms $Ar_2(^3\Sigma_u^+)$ by the three-body reaction (16). Although $Ar_2(^3\Sigma_u^+)$ contributes to NO dissociation (19), $Ar_2(^3\Sigma_u^+)$ is quenched by CO in a parallel reaction (53). Therefore, at low CO concentrations, the quenching rate of $Ar_2(^3\Sigma_u^+)$ with CO (53) increases with increasing CO concentration at the expense of NO conversion, which leads to less NO dissociation by $Ar_2(^3\Sigma_u^+)$ by (19) and explains the initial decrease of NO

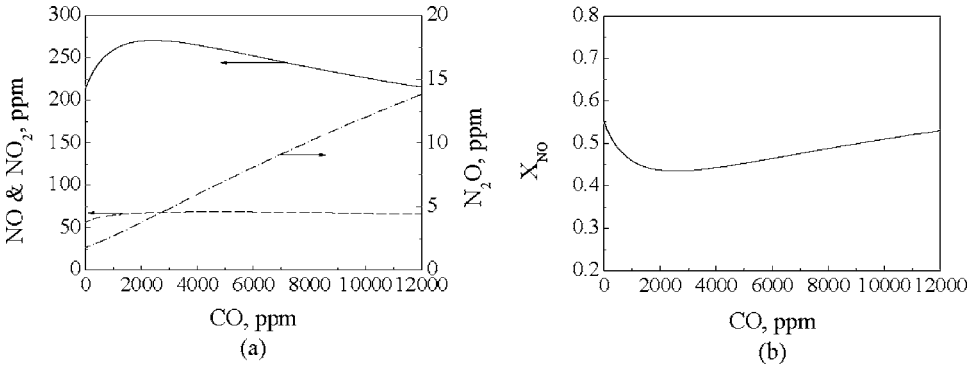

FIG. 10. Model prediction of CO effect on NO conversion at a flow rate of 4.01×10^{-4} m^3 s^{-1} and 189 kPa. Power input: 60 W; inlet NO concentration: 600 ppm. (a) NO, NO_2, and N_2O concentrations as a function of CO concentration: (—) NO, (---) NO_2, and (---) N_2O. (b) Conversion of NO and NO_2 as a function of CO concentration.

conversion with increasing CO concentrations below ~2400 ppm.

With further increases in CO concentration above ~2400 ppm, CO dissociation (52) gradually becomes prominent, resulting in increasing NO conversion through atomic C. C is a very active radical that can convert NO to form the radicals, CN (63) and N (64), and reacts with CO to form C_2O (67). CN converts NO in (74) and reacts with NO_2 to form NCO (75), while N converts NO in (24). C_2O reacts with NO to form additional CN (69) and NCO (68). Finally, NCO converts NO in reactions (82) and (83). The net result is that one atomic C radical can convert three NO molecules, which causes NO conversion to increase from the minimum at CO concentrations of ~2400 ppm.

The rate of increase in NO conversion is low for the following reasons. (1) As noted above, with increasing CO concentration, additional $Ar_2(^3\Sigma_u^+)$ formed by (16) is largely quenched by CO (53) and hence does not contribute to NO conversion (19). For example, NO conversion selectivity (S_{r,NO_x}) decreases from 39.1% without CO (Table II) to 27.6% at 1.01% CO (Table III). (2) Similarly, the contribution of $Ar(^3P_2)$ to NO dissociation (10) also decreases with increasing CO concentration, as noted previously. (3) Although one atomic C radical can convert three NO molecules, the effect just slightly exceeds the decreasing rate of NO dissociation through (10) because the rate constant of CO dissociation (52) is nearly one order of magnitude lower than the rate constant of (10). As a result, NO conversion slowly returns from the minimum reached at ~2400 ppm CO to approximately the same level at 1.01% CO concentration as the NO conversion observed in the absence of CO [as shown in Figs. 1(c) and 1(d) and Figs. 10(a) and 10(b)].

The linear increase in N_2O concentration with increasing CO concentration [Fig. 10(a)] occurs because C radicals contribute to NCO formation through (68), (70), (75), and (79) and NCO reacts with NO to form N_2O (82). The destruction rate of N_2O by (12), (21), (38), and (65) is very slow because the N_2O concentration is low (less than 26 ppm, as shown in Fig. 7).

Figure 11 shows a calculated example of the effect of CO on 200 ppm N_2O conversion in Ar for CO concentrations ranging from 0 to 12 000 ppm, at a total flow rate of 4.01×10^{-4} m^3 s^{-1} and 189 kPa, constant power input of 60 W, and the same model parameters α_2 and β_2. Similar results are obtained at other conditions. Figure 11 suggests that N_2O concentration increases with increasing CO concentration, corresponding to decreasing N_2O conversion with increasing CO concentration. Therefore, CO inhibits N_2O conversion, which is consistent with the experimental observation shown in Figs. 2(a) and 2(b). N_2O conversion decreases toward an asymptotic value with increasing CO concentration.

Although the effects of CO on NO conversion and on N_2O conversion are qualitatively different (Figs. 10 and 11), the N_2O conversion trends in Fig. 11 can be explained by the same reaction mechanism as that used to explain the NO conversion trend (Table IV); that is, both $Ar(^3P_2)$ and $Ar_2(^3\Sigma_u^+)$ contribute to N_2O conversion in the absence of CO as follows:

$$Ar(^3P_2) + N_2O \rightarrow Ar + N_2(B) + O,$$

$$k = 2.65\times10^{14}\ \text{cm}^3\ \text{mol}^{-1}\ \text{s}^{-1} \qquad (12')$$

$$Ar_2(^3\Sigma_u^+) + N_2O \rightarrow 2Ar + N_2 + O,$$

$$k = 3.31\times10^{14}\ \text{cm}^3\ \text{mol}^{-1}\ \text{s}^{-1}. \qquad (21')$$

At low CO concentrations, most $Ar(^3P_2)$ form $Ar_2(^3\Sigma_u^+)$ by the three-body reaction (16) (Table II) discussed previously, which further contributes to N_2O dissociation in (21). However, $Ar_2(^3\Sigma_u^+)$ is quenched by CO in (53). Therefore, at low CO concentrations, N_2O conversion decreases quickly with increasing CO concentration. With further increases in CO concentration, the CO dissociation reaction (52) gradually becomes prominent. Atomic C can dissociate N_2O in (65). Therefore, N_2O conversion initially decreases rapidly, and then above approximately 5000 ppm CO, N_2O conversion

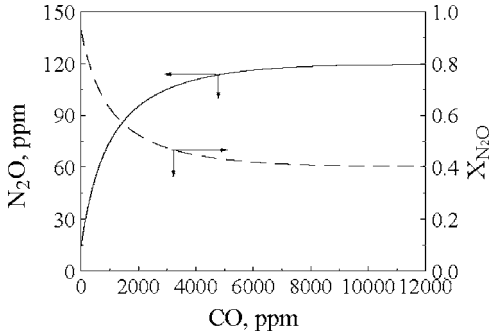

FIG. 11. Model prediction of CO effect on N_2O conversion at a flow rate of 4.01×10^{-4} m^3 s^{-1} and 189 kPa. Power input: 60 W; inlet N_2O concentration: 200 ppm. (—) N_2O concentration; (---) N_2O conversion.

decreases slowly with increasing CO concentration, as shown in Fig. 11. However, unlike NO conversion, the radicals resulting from atomic C, such as CN, C_2O, and NCO, do not convert N_2O. As a result, the reaction rate of atomic C with CO (67) increases with increasing CO concentration and fewer C radicals are available to dissociate N_2O, leading to the continued decrease of N_2O conversion with further increases in CO concentration.

IV. SUMMARY

CO concentrations of 200–600 ppm inhibit NO conversion in nonthermal Ar plasma. N_2O is not detectable. CO concentrations of 1.01% have no effect on NO conversion, but N_2O is detected. N_2O conversion in Ar plasma decreases with increasing CO concentration. Selectivity analysis of the Ar excited states likely to contribute to NO_x conversion without and with CO suggests that $Ar(^3P_2)$ rather than Ar^+ is the only active species that contributes significantly to NO_x conversion and CO dissociation. Other excited states of Ar are predominantly quenched by Ar and CO, or radiatively decay to ground states. A kinetic model including 43 reactions is required to model NO or N_2O conversion in Ar without CO, whereas 81 reactions are required to model NO or N_2O conversion in Ar with CO. At constant gas pressure, a single set of model parameters can predict both NO conversion and N_2O conversion without and with CO. The analysis explains all experimental observations on the effect of CO on NO and N_2O conversions in nonthermal Ar plasma. Reaction mechanisms including Ar^+ cannot provide a reasonable explanation for these experimental data.[11] The experimental results can be explained by invoking the reaction mechanism including the excited states of Ar, which supports the conclusion that cations have a negligible contribution to the nonthermal plasma reaction.

ACKNOWLEDGMENTS

This work was funded by the Department of Defense (ARO-DAAD19-01-1-0488) and the National Science Foundation (CTS-9810040 and CTS-0078700). The matching support was provided by the Research Office, University of Wyoming. The authors gratefully acknowledge experimental assistance provided by Dr. X. Hu, S. V. B. Janardhan Garikipati, Dr. S. Legowski, and R. Borgialli.

[1] J. S. Chang, J. Aerosol Sci. **20**, 1087 (1989).
[2] U. Kogelschatz, Plasma Chem. Plasma Process. **23**, 1 (2003).
[3] E. M. van Veldhuizen, W. R. Rutgers, and V. A. Bityurin, Plasma Chem. Plasma Process. **16**, 227 (1996).
[4] X. Hu, J.-J. Zhang, S. Mukhnahallipatna, J. Hamann, M. J. Biggs, and P. Agarwal, Fuel **82**, 1675 (2003).
[5] G.-B. Zhao, X. Hu, M. D. Argyle, and M. Radosz, Ind. Eng. Chem. Res. **43**, 5077 (2004).
[6] G.-B. Zhao, X. Hu, M. C. Yeung, O. A. Plumb, and M. Radosz, Ind. Eng. Chem. Res. **43**, 2315 (2004).
[7] G.-B. Zhao, S. V. B. J. Garikipati, X. Hu, M. D. Argyle, and M. Radosz, AIChE J. **51**, 1800 (2005).
[8] G.-B. Zhao, X. Hu, M. D. Argyle, and M. Radosz, Ind. Eng. Chem. Res. **44**, 3925 (2005).
[9] G.-B. Zhao, X. Hu, M. D. Argyle, and M. Radosz, Ind. Eng. Chem. Res. **44**, 3935 (2005).
[10] G.-B. Zhao, M. D. Argyle, and M. Radosz, J. Appl. Phys. (submitted).
[11] X. Hu, G.-B. Zhao, J.-J. Zhang, L. Wang, and M. Radosz, Ind. Eng. Chem. Res. **43**, 7456 (2004).
[12] G.-B. Zhao, X. Hu, and M. Radosz, The Army Research Office Report No. DADD19-01-1-048, 2004 (unpublished).
[13] G.-B. Zhao, X. Hu, O. A. Plumb, and M. Radosz, Energy Fuels **18**, 1522 (2004).
[14] G.-B. Zhao, S. V. B. J. Garikipati, X. Hu, M. D. Argyle, and M. Radosz, Chem. Eng. Sci. **60**, 1927 (2005).
[15] G.-B. Zhao, S. V. B. J. Garikipati, X. Hu, M. D. Argyle, and M. Radosz, AIChE J. **51**, 1813 (2005).
[16] G. E. Vogtlin, in *Non-Thermal Plasma Techniques for Pollution Control: Electron Beam and Electrical Discharge*, edited by B. M. Penetrante and S. E. Schultheis (Springer-Verlag, Berlin, Heidelberg, 1993), Vol. G34, Part B, pp. 187–198.
[17] K. Schofield, J. Phys. Chem. Ref. Data **8**, 723 (1979).
[18] J. A. Kerr, in *CRC Handbook of Chemistry and Physics*, edited by D. R. Lide (CRC, Boca Raton, FL, 2003), pp. 9–56.
[19] J. W. Keto and C.-Y. Kuo, J. Chem. Phys. **74**, 6188 (1981).
[20] R. S. F. Chang and D. W. Setser, J. Chem. Phys. **69**, 3885 (1978).
[21] J. H. Kolts and D. W. Setser, J. Chem. Phys. **68**, 4848 (1978).
[22] P. Moutard, P. Laporte, J.-L. Subtil, N. Damany, and H. Damany, J. Chem. Phys. **87**, 4576 (1987).
[23] J. Balamuta and M. F. Golde, J. Phys. Chem. **86**, 2765 (1982).
[24] J. Balamuta and M. F. Golde, J. Chem. Phys. **76**, 2430 (1982).
[25] M. J. Kiik, P. Dubé, and B. P. Stoicheff, J. Chem. Phys. **102**, 2351 (1995).
[26] R. Mehnert, O. Brede, and R. Hermann, Radiat. Phys. Chem. **28**, 455 (1986).
[27] T. Oka, M. Kogoma, M. Imamura, S. Arai, and T. Watanabe, J. Chem. Phys. **70**, 3384 (1979).
[28] M. T. Jones, T. D. Dreiling, D. W. Setser, and R. N. McDonald, J. Phys. Chem. **89**, 4501 (1985).
[29] G. W. Tyndall, M. S. De Vries, C. L. Cobb, and R. M. Martin, J. Chem. Phys. **87**, 5830 (1987).
[30] M. P. Skrzypkowski, R. Johnsen, R. E. Rosati, and M. F. Golde, Chem. Phys. **296**, 23 (2004).
[31] K. Tachibana, Phys. Rev. A **34**, 1007 (1986).
[32] G. A. Piech, J. B. Boffard, M. F. Gehrke, L. W. Anderson, and C. C. Lin, Phys. Rev. Lett. **81**, 309 (1998).
[33] Y. Itikawa *et al.*, J. Phys. Chem. Ref. Data **15**, 985 (1986).
[34] W. L. Wiese, J. W. Brault, K. Danzmann, V. Helbig, and M. Kock, Phys. Rev. A **39**, 2461 (1989).
[35] N. E. Small-Warren and L.-Y. C. Chiu, Phys. Rev. A **11**, 1777 (1975).
[36] H. Katori and F. Shimizu, Phys. Rev. Lett. **70**, 3545 (1993).
[37] E. Ellis and N. D. Twiddy, J. Phys. B **2**, 1366 (1969).
[38] J. B. Boffard, G. A. Piech, M. F. Gehrke, L. W. Anderson, and C. C. Lin, Phys. Rev. A **59**, 2749 (1999).
[39] J. E. Velazco, J. H. Kolts, and D. W. Setser, J. Chem. Phys. **69**, 4357 (1978).
[40] N. Sadeghi, D. W. Setser, A. Francis, U. Czarnetzki, and H. F. Döbele, J. Chem. Phys. **115**, 3144 (2001).
[41] K. T. Wu, J. Phys. Chem. **92**, 2657 (1988).
[42] F. Collier, J. B. Leblond, F. Hoffbeck, and P. Cottin, J. Chem. Phys. **74**, 4372 (1981).
[43] R. Atkinson, D. L. Baulch, R. A. Cox, J. R. F. Hampson, J. A. Kerr, and J. Troe, J. Phys. Chem. Ref. Data **18**, 881 (1989).
[44] I. A. Kossyi, A. Y. Kostinsky, A. A. Matveyev, and V. P. Silakov, Plasma Sources Sci. Technol. **1**, 207 (1992).
[45] H. Matzing, in *Advances in Chemical Physics*, edited by I. Prigogine and S. A. Rice (Wiley, New york, 1991), Vol. LXXX, pp. 315–402.
[46] G. Yarwood, J. W. Sutherland, M. A. Wickramaaratchi, and R. B. Klemm, J. Phys. Chem. **95**, 8771 (1991).
[47] R. Atkinson, D. L. Baulch, R. A. Cox, J. R. F. Hampson, J. A. Kerr, M. J. Rossi, and J. Troe, J. Phys. Chem. Ref. Data **26**, 1329 (1997).
[48] W. Tsang and R. F. Hampson, J. Phys. Chem. Ref. Data **15**, 1087 (1986).
[49] J. T. Herron, J. Phys. Chem. Ref. Data **28**, 1453 (1999).
[50] J. T. Herron and D. S. Green, Plasma Chem. Plasma Process. **21**, 459 (2001).
[51] A. Lofthus and P. H. Krupenie, J. Phys. Chem. Ref. Data **6**, 113 (1977).
[52] E. Gat, N. Gherardi, S. Lemoing, F. Massines, and A. Ricard, Chem. Phys. Lett. **306**, 263 (1999).
[53] L. G. Piper, J. Chem. Phys. **91**, 864 (1989).
[54] R. A. Young, G. Black, and T. G. Slanger, J. Chem. Phys. **50**, 303 (1969).
[55] L. G. Piper, J. Chem. Phys. **97**, 270 (1992).
[56] J. Henriques, E. Tatarova, V. Guerra, and C. M. Ferreira, J. Appl. Phys. **91**, 5622 (2002).

[57]S. V. Pancheshnyi, S. M. Starikovskaia, and A. Y. Starikovskii, Chem. Phys. Lett. **294**, 523 (1998).
[58]A. Cenian, A. Chernukho, and V. Borodin, Contrib. Plasma Phys. **35**, 273 (1995).
[59]D. H. Stedman and D. W. Setser, Prog. React. Kinet. **6**, 193 (1971).
[60]F. Albugues, A. Birot, D. Blanc, H. Brunet, J. Galy, P. Millet, and J. L. Teyssier, J. Chem. Phys. **61**, 2695 (1974).
[61]S. Andersson, N. Markovic, and G. Nyman, J. Phys. Chem. A **107**, 5439 (2003).
[62]G. Dorthe, P. Caubet, T. Vias, B. Barrere, and J. Marchais, J. Phys. Chem. **95**, 5109 (1991).
[63]D. Chastaing, P. L. James, I. R. Sims, and I. W. M. Smith, Phys. Chem. Chem. Phys. **1**, 2247 (1999).
[64]W. D. Thweatt, M. A. Erickson, and J. F. Hershberger, J. Phys. Chem. A **108**, 74 (2004).
[65]K. H. Becker, R. König, R. Meuser, P. Wiesen, and K. D. Bayes, J. Photochem. Photobiol., A **64**, 1 (1992).
[66]B. Brunetti and G. Liuti, Z. Phys. Chem., Neue Folge **94**, 19 (1975).
[67]G. Dorthe, in *N-Centered Radicals*, edited by Z. B. Alfassi (Wiley, Chichester, UK, 1998), pp. 1–37.
[68]J. Park and J. F. Hershberger, J. Chem. Phys. **99**, 3488 (1993).
[69]W. F. Cooper, J. Park, and J. F. Hershberger, J. Phys. Chem. **97**, 3283 (1993).
[70]G. Black, L. E. Jusinski, M. R. Taherian, T. G. Slanger, and D. L. Huestis, J. Phys. Chem. **90**, 6842 (1986).
[71]W. Tsang, J. Phys. Chem. Ref. Data **21**, 753 (1992).
[72]R. A. Brownsword, G. Hancock, and D. E. Heard, J. Chem. Soc., Faraday Trans. **93**, 2473 (1997).